Inhomogeneous magnetization in dipolar ferromagnetic liquids

B. Groh and S. Dietrich
Fachbereich Physik, Bergische Universität Wuppertal, D-42097 Wuppertal, Federal Republic of Germany
(Received 3 December 1997)

At high densities fluids of strongly dipolar spherical particles exhibit spontaneous long-ranged orientational order. Typically, due to demagnetization effects induced by the long range of the dipolar interactions, the magnetization structure is spatially inhomogeneous and depends on the shape of the sample. We determine this structure for a cubic sample by the free minimization of an appropriate microscopic density functional using simulated annealing. We find a vortex structure resembling four domains separated by four domain walls whose thickness increases proportional to the system size L. There are indications that for large L the whole configuration scales with the system size. Near the axis of the mainly planar vortex structure the direction of the magnetization escapes into the third dimension or, at higher temperatures, the absolute value of the magnetization is strongly reduced. Thus the orientational order is characterized by two point defects at the top and the bottom of the sample, respectively. The equilibrium structure in an external field and the transition to a homogeneous magnetization for strong fields are analyzed, too. [S1063-651X(98)12604-1]

PACS number(s): 75.50.Mm, 64.70.−p, 75.70.Kw, 61.30.Cz

I. INTRODUCTION

At high densities strongly dipolar fluids can exhibit an orientationally ordered liquid phase characterized by a spontaneous magnetization. This has been demonstrated for the first time by Monte Carlo simulations of dipolar soft spheres by Wei and Patey [1,2] and has been confirmed by simulations of hard spheres [3–5] and of Stockmayer fluids [6]. Theoretical approaches leading to the same conclusion include a mean-field theory for a dipolar lattice gas [7], a generalized van der Waals theory [8], and different kinds of density-functional theory [9–11]. At low densities the typical configurations of dipolar fluids exhibit chain formation [12–14,5], which may inhibit the phase transition from the isotropic vapor phase to the isotropic liquid phase [15–18]. If the dipole moments are *electric* as in molecular liquids the orientationally ordered phase exhibits a spontaneous polarization; in the case of *magnetic* dipoles as in ferrofluids, i.e., colloidal suspensions of permanently ferromagnetic particles, one speaks of ferromagnetic order and a spontaneous magnetization. In this paper we adopt the magnetic language, keeping in mind that completely analogous phenomena occur in the electric case (as long as no free charge carriers are present in the fluid).

In both simulations and analytic theories the dipolar forces must be treated carefully due to their long range, which may give rise to effects depending on the shape of the sample. It turns out that for all sample shapes with the exception of a long needle the equilibrium configuration is inhomogeneous with a spatially varying magnetization $\mathbf{M}(\mathbf{r})$ [19,20]. This leads to a shape *independent* free energy, as is expected on general grounds [21]. The highly nontrivial problem to determine explicitly the spatial distribution of this inhomogeneous magnetization for a given sample shape has not yet been solved satisfactorily. In simulations usually a homogeneous magnetization is enforced by using an infinitely permeable surrounding of the periodically repeated simulation cells. If instead the sample is surrounded by vacuum the simulation cell splits into two domains with opposing magnetizations [2]. But this structure is clearly induced by the artificial periodic boundary conditions. We addressed this problem recently [20] for the experimentally more relevant case of open boundaries and obtained the following general characterization of the equilibrium configurations: On a macroscopic scale the absolute value of $\mathbf{M}(\mathbf{r})$ is constant, its divergence is zero, and at the surfaces the normal component vanishes. However, these properties do not yet enable one to construct the configuration for a given shape. For a cubic sample we determined [20] the most stable configuration under the constraint of sharp domain boundaries. It consists of four triangular domains with 90° domain walls in between. In contrast to solid ferromagnets the number of domains does not increase with the system size, but remains as small as possible. On the other hand the assumption of sharp domain boundaries is not justified for liquid systems. Due to the lack of a lattice anisotropy one rather expects very thick domain walls [22].

Therefore, in order to analyze the domain configuration in more detail in the present work we have performed a numerical minimization of an approximate microscopic density functional that has been used before [10,11,20] to describe the ferromagnetically ordered fluid. We have made no *a priori* assumptions regarding the symmetry of the domain structure and have minimized with respect to a large number $(10^4–10^5)$ of parameters that represent the local magnetization at mesh points within the sample. This approach is similar in spirit to the determination of the magnetization structure of solid ferromagnetic particles of micrometer size in the framework of micromagnetic theory [23–25]. But there are two main differences. First, we do not constrain the absolute value of the magnetization, thus allowing for the formation of less ordered regions. Second, we work on the microscopic scale determined by the particle diameter, which enables us to examine in detail the overall structure as well as the structure of domain walls and the cores of topological defects.

A brief account of some of our results has been published

in Ref. [26]. Here we provide the important derivation of the functional from the underlying model, discuss the implementation of the simulated annealing, and give a thorough analysis of the resulting configurations. We also analyze the consequences of the necessary discretization and of the finite sample size. Furthermore we discuss in detail the orientational structure in an external field, which is relevant for the experiments with the recently discovered metallic liquid ferromagnets [27–29].

II. MODEL AND THEORETICAL APPROACH

A. Density-functional theory for Stockmayer fluids

We consider Stockmayer fluids consisting of spherical particles with fixed embedded point dipoles that interact via pairwise dispersion and dipolar forces. The interaction potential $w=w_{\mathrm{LJ}}+w_{\mathrm{dip}}$ is the sum of the Lennard-Jones potential

$$w_{\mathrm{LJ}}(r_{12})=4\epsilon\left[\left(\frac{\sigma}{r_{12}}\right)^{12}-\left(\frac{\sigma}{r_{12}}\right)^{6}\right] \tag{1}$$

and the dipolar potential

$$w_{dip}(\mathbf{r}_{12},\omega,\omega')=\frac{m^2}{r_{12}^3}[\hat{\mathbf{m}}(\omega)\cdot\hat{\mathbf{m}}(\omega')-3(\hat{\mathbf{m}}(\omega)\cdot\hat{\mathbf{r}}_{12})\times(\hat{\mathbf{m}}(\omega')\cdot\hat{\mathbf{r}}_{12})]\Theta(r_{12}-\sigma). \tag{2}$$

$\mathbf{r}_{12}=\mathbf{r}-\mathbf{r}'=r_{12}\hat{\mathbf{r}}_{12}$ denotes the interparticle vector, $\omega=(\theta,\phi)$ and ω' are the orientations of the dipole moments at $\mathbf{r}$ and $\mathbf{r}'$, respectively, with $m=|\mathbf{m}|$; carets indicate unit vectors. At short distances the interaction is cut off by the Heaviside function Θ.

In order to study the spatially inhomogeneous configurations within a ferromagnetically ordered fluid we employ the density-functional theory introduced in Ref. [30] and for which we have worked out analytical results previously [10,11,20].

The configurations of the fluid are described by the spatially constant number density ρ and the normalized orientational distribution $\alpha(\mathbf{r},\omega)$ so that the probability density for finding a particle at point $\mathbf{r}$ with the orientation ω is $\hat{\rho}(\mathbf{r},\omega)=\rho\alpha(\mathbf{r},\omega)$. The free energy density functional is given by

$$F(\rho,[\alpha(\mathbf{r},\omega)];T)=Vf_{\mathrm{HS}}(\rho,T)+F_{\mathrm{or}}+F_{\mathrm{ex}}+F_H. \tag{3}$$

V is the sample volume and f_{HS} is the free energy density of the hard sphere reference system characterized by an effective temperature dependent radius [30]. The second term $[\beta=1/(k_BT)]$,

$$F_{\mathrm{or}}=\frac{\rho}{\beta}\int_V d^3r\int d\omega\,\alpha(\mathbf{r},\omega)\ln[4\pi\alpha(\mathbf{r},\omega)], \tag{4}$$

takes into account the loss of entropy if the orientational distribution is not isotropic, i.e., different from $1/(4\pi)$. Here and in the following the integrations over the angles ω are taken over the unit sphere. For the excess contribution F_{ex} due to the long-ranged part of the interaction potential we apply the low-density approximation for the pair distribution function, which yields [30]

$$F_{\mathrm{ex}}=-\frac{\rho}{2\beta}\int_V d^3r\int_V d^3r'\int d\omega d\omega'\,\alpha(\mathbf{r},\omega)\alpha(\mathbf{r}',\omega')\times\Theta(r_{12}-\sigma)\tilde{f}(\mathbf{r}_{12},\omega,\omega') \tag{5}$$

with the Mayer function

$$\tilde{f}(\mathbf{r}_{12},\omega,\omega')=-1+\exp[-\beta w(\mathbf{r}_{12},\omega,\omega')]. \tag{6}$$

We regard this approximation as a first step towards an analytic quantitative theory of dipolar liquids. Improvements that employ pair distribution functions obtained from integral equation theories have been worked out for homogeneous dipolar fluids [31] but are numerically too demanding for the inhomogeneous case examined here.

The Mayer function in Eq. (6) can be expanded in terms of the rotational invariants [$C(l_1l_2l,m_1m_2m)$ are Clebsch-Gordan coefficients]

$$\Phi_{l_1l_2l}(\omega,\omega',\omega_{12})=\sum_{m_1,m_2,m}C(l_1l_2l,m_1m_2m)\times Y_{l_1m_1}(\omega)Y_{l_2m_2}(\omega')Y^*_{lm}(\omega_{12}) \tag{7}$$

with coefficients $\hat{f}$ depending only on the distance between the particles:

$$\tilde{f}(\mathbf{r}_{12},\omega,\omega')=\sum_{l_1l_2l}\hat{f}_{l_1l_2l}(r_{12})\Phi_{l_1l_2l}(\omega,\omega',\omega_{12}). \tag{8}$$

Finally, the interaction energy with a homogeneous external field H is

$$F_H=-\rho mH\int_V d^3r\int d\omega\,\alpha(\mathbf{r},\omega)\cos\gamma, \tag{9}$$

where γ is the angle between ω and the direction of the field. We take into account the external potential due to the container walls only summarily in that they provide the confinement of the fluid to V because we are interested in the *bulk* behavior of the fluid. In this spirit we also do not consider spatial variations of the number density $\rho(\mathbf{r})=\int d\omega\hat{\rho}(\mathbf{r},\omega)$ in the vicinity of the walls. Moreover, in Eqs. (3)–(9) we have assumed that $\rho(\mathbf{r})$ is constant throughout the sample even if $\alpha(\mathbf{r},\omega)$ varies deep inside the sample. We expect that due to the small compressibility of the fluid in the orientationally ordered phase possible variations of $\rho(\mathbf{r})$, e.g., inside the domain walls, are only small and thus not significant.

In the next step the orientational distribution is expanded into spherical harmonics:

$$\alpha(\mathbf{r},\omega)=\sum_{l=0}^{\infty}\sum_{m=-l}^{l}\mu_{lm}(\mathbf{r})Y_{lm}(\omega) \tag{10}$$

with $\mu_{00}=1/\sqrt{4\pi}$ due to the normalization $\int d\omega\alpha(\mathbf{r},\omega)=1$ and $\mu_{lm}^{*}=(-1)^{m}\mu_{l,-m}$ because α is real. Inserting Eqs. (8) and (10) into Eq. (5) one finds for the excess free energy

$$F_{\mathrm{ex}}=-\frac{\rho^{2}}{2\beta}\sum_{l_1,l_2,l}\sum_{m_1,m_2,m}C(l_1l_2l,m_1m_2m)\times\int_V d^3r\int_V d^3r'\,\mu_{l_1m_1}(\mathbf{r})\mu_{l_2m_2}(\mathbf{r}')\hat{f}_{l_1l_2l}(r_{12})Y_{lm}(\omega_{12}). \tag{11}$$

In order to make the free minimization of the density functional with respect to the set $\{\mu_{lm}(\mathbf{r})\}$ numerically feasible we must refrain from determining the full orientational distribution $\alpha(\mathbf{r},\omega)$ at each point $\mathbf{r}$. Instead we focus on the reduced information provided by the dimensionless local magnetization

$$\mathbf{M}(\mathbf{r})=\int d\phi d\theta\,\sin\theta\alpha(\mathbf{r},\omega)\begin{pmatrix}\cos\phi\,\sin\theta\\ \sin\phi\,\sin\theta\\ \cos\theta\end{pmatrix}=\begin{pmatrix}-\sqrt{2}\,\mathrm{Re}\mu_{11}(\mathbf{r})\\ \sqrt{2}\,\mathrm{Im}\mu_{11}(\mathbf{r})\\ \mu_{10}(\mathbf{r})\end{pmatrix}=\begin{pmatrix}M_1(\mathbf{r})\\ M_2(\mathbf{r})\\ M_3(\mathbf{r})\end{pmatrix}. \tag{12}$$

[The actual magnetization is $\mathcal{M}(\mathbf{r})=\sqrt{4\pi/3}\rho m\mathbf{M}(\mathbf{r})$.] Thus $\mathbf{M}(\mathbf{r})$ can be obtained from the orientational distribution $\alpha(\mathbf{r},\omega)$ and denotes the spatially varying *thermal average* of the fluctuating dipole moment. The above restriction implies that in Eq. (10) only terms up to $l=1$ have to be taken into account. Within this approximation those contributions to the excess free energy which depend on the orientational order are given by

$$\begin{aligned}\Delta F_{\mathrm{ex}}&=F_{\mathrm{ex}}^{(110)}+F_{\mathrm{ex}}^{(112)}\\&=\frac{\rho^{2}}{2\beta}\frac{1}{\sqrt{12\pi}}\int_V d^3r\int_V d^3r'\mathbf{M}(\mathbf{r})\cdot\mathbf{M}(\mathbf{r}')\times\Theta(r_{12}-\sigma)\hat{f}_{110}(r_{12})\\&\quad+\frac{\rho^{2}}{2\beta}\sqrt{\frac{5}{24\pi}}\int_V d^3r\int_V d^3r'\mathbf{M}(\mathbf{r})\hat{\mathbf{T}}(\hat{\mathbf{r}}_{12})\mathbf{M}(\mathbf{r}')\times\Theta(r_{12}-\sigma)\hat{f}_{112}(r_{12})\end{aligned} \tag{13}$$

with the tensor $\hat{T}_{ij}(\hat{\mathbf{r}})=\delta_{ij}-3\hat{r}_i\hat{r}_j$. We note that in contrast to Ref. [20] we do not have to separate long- and short-ranged contributions to $\hat{f}_{112}$ because within our numerical approach we are always dealing with finite systems without carrying out the thermodynamic limit. Analytic expressions for the functions $\hat{f}_{11l}$ are provided by Eqs. (B33) and (B34) in Ref. [30] from which one obtains the following expansions in terms of m^2:

$$\hat{f}_{110}(r)=-\frac{8\pi}{25}\sqrt{\frac{4\pi}{3}}e^{-\beta w_{\mathrm{LJ}}(r)}\frac{\beta^3m^6}{r^9}+O(m^{10}), \tag{14}$$

$$\hat{f}_{112}(r)=(4\pi)^{3/2}\sqrt{\frac{2}{15}}\left[(1-e^{-\beta w_{\mathrm{LJ}}(r)})\frac{\beta m^2}{r^3}+\frac{6}{25}e^{-\beta w_{\mathrm{LJ}}(r)}\frac{\beta^3m^6}{r^9}+O(m^{10})\right].$$

To lowest order in m^2 the function $\hat{f}_{112}(r)$ contains the characteristic dependence $\sim r^{-3}$ of the dipolar potential whereas the function $\hat{f}_{110}$ arises only due to the cubic and higher order terms in the expansion of the Mayer function. [For the actual calculations we have used the full expressions as given in Ref. [30] instead of the expansions in Eq. (14).]

In the following we specifically analyze a cubic volume of side length L containing the fluid. The spatial integrations are discretized by introducing a (simple cubic) lattice with lattice constant $a=L/N$ and lattice vectors $\mathbf{R}=a(n_1,n_2,n_3)$, with $n_i\in\{-(N-1)/2,\ldots,-\frac{1}{2},\frac{1}{2},\ldots,(N-1)/2\}$ (N is even), so that

$$\Delta F_{\mathrm{ex}}=\frac{\rho^{2}}{2\beta}a^6\sum_{\mathbf{R}}\sum_{\mathbf{R}'}\sum_{i,j}M_i(\mathbf{R})w_{ij}(\mathbf{R}-\mathbf{R}')M_j(\mathbf{R}'). \tag{15}$$

The interaction tensor w_{ij} is given by

$$w_{ij}(\mathbf{R})=\sqrt{\frac{5}{24\pi}}\Theta(R-\sigma)\left[\sqrt{\frac{2}{5}}\hat{f}_{110}(R)\delta_{ij}+\hat{f}_{112}(R)(\delta_{ij}-3\hat{R}_i\hat{R}_j)\right],\quad i,j=1,2,3, \tag{16}$$

so that $w_{ij}(-\mathbf{R})=w_{ij}(\mathbf{R})$. (The value of σ/a is taken to be noninteger; otherwise there are distances between lattice points that correspond to the discontinuity of the Heaviside function.) An alternative formulation, which will prove to be helpful later on, is

$$\Delta F_{\mathrm{ex}}=\frac{\rho^{2}}{2\beta}a^3\sum_{\mathbf{R}}\sum_{i}H_i(\mathbf{R})M_i(\mathbf{R}) \tag{17}$$

with the local fields

$$H_i(\mathbf{R})=a^3\sum_{\mathbf{R}'}\sum_{j}w_{ij}(\mathbf{R}-\mathbf{R}')M_j(\mathbf{R}'). \tag{18}$$

The entropic term given by Eq. (4) can be simplified using the fact that by applying a suitable rotation the orientational distribution at a given point $\mathbf{r}$ can be cast into the form

$$\alpha(\mathbf{r},\omega)=\frac{1}{4\pi}+M(\mathbf{r})\sqrt{\frac{3}{4\pi}}\cos\theta \tag{19}$$

with $M(\mathbf{r})=|\mathbf{M}(\mathbf{r})|$. Due to the angular integration in Eq. (4) this rotation does not alter the value of F_{or} so that

$$F_{\rm or}=\frac{\rho}{\beta}\int_V d^3r\int d\omega\left(\frac{1}{4\pi}+M(\mathbf{r})\sqrt{\frac{3}{4\pi}}\cos\theta\right)$$
$$\times\ln(1+M(\mathbf{r})\sqrt{12\pi}\cos\theta). \tag{20}$$

The expansion of the logarithm yields in the discrete version

$$F_{\rm or}=\frac{\rho}{\beta}a^3\sum_{\mathbf{R}}\sum_{n=1}^{\infty}\frac{[\sqrt{12\pi}M(\mathbf{R})]^{2n}}{(2n-1)2n(2n+1)}$$
$$=\frac{\rho}{\beta}a^3\sum_{\mathbf{R}}s(M(\mathbf{R})). \tag{21}$$

Finally, the term due to the external field, which is taken to point into the z direction, is

$$F_H=-\sqrt{\frac{4\pi}{3}}\rho mHa^3\sum_{\mathbf{R}}M_3(\mathbf{R}). \tag{22}$$

Thus the free energy difference F_{if} between the ferromagnetic and the isotropic phases is

$$F_{if}=F_{\rm or}+\Delta F_{\rm ex}+F_H, \tag{23}$$

where the individual terms are given by Eqs. (15), (21), and (22), respectively.

B. Simulated annealing

We have minimized the free energy in Eq. (23) with respect to the magnetization configuration $\{\mathbf{M}(\mathbf{R})\}$ by using the simulated annealing algorithm [32]. In the first step the interaction tensor w_{ij} is determined once for all relevant distances between the lattice sites within $V=L^3$. In the second step the local fields $H_i(\mathbf{R})$ are calculated for an initial choice of the configuration $\mathbf{M}^{(\rm ini)}(\mathbf{R})$ according to Eq. (18). In each following step a lattice site $\mathbf{R}_0$ is chosen and a new magnetization $\mathbf{M}'(\mathbf{R}_0)$ is proposed by changing each component $i=1,2,3$ by a random value $\Delta M_i=M_i'(\mathbf{R}_0)-M_i(\mathbf{R}_0)$ between $-\kappa M(\mathbf{R}_0)$ and $+\kappa M(\mathbf{R}_0)$ ($\kappa=0.1$ turned out to be a suitable choice). The resulting change in free energy is

$$\Delta F_{if}=\frac{\rho}{\beta}a^3\left[s(M'(\mathbf{R}_0))-s(M(\mathbf{R}_0))+\sum_i H_i(\mathbf{R}_0)\Delta M_i\right]$$
$$-\sqrt{\frac{4\pi}{3}}\rho mHa^3\Delta M_3. \tag{24}$$

There is no term quadratic in ΔM_i due to $w_{ij}(\mathbf{R}=0)=0$. The proposed change of the configuration is accepted with certainty if ΔF_{if} is negative and with a probability $\exp[-\Delta F_{if}/(k_BT_s)]$ if it is positive. T_s is the control temperature of the annealing algorithm, which is decreased slowly during the minimization. In case of acceptance the new field $H_i'(\mathbf{R})$ at each site is calculated according to [see Eq. (18)]

$$H_i'(\mathbf{R})=H_i(\mathbf{R})+a^3\sum_j w_{ij}(\mathbf{R}-\mathbf{R}_0)\Delta M_j. \tag{25}$$

The time required for this computational step, which is consuming most of the CPU time, is of the order $O(N^3)$. The advantage of using the local fields is that they need not be updated if the proposed change is rejected, which happens quite often especially at low control temperatures near the end of a run, while the acceptance decision itself can be reached very fast.

The control temperature is lowered by a factor of 0.95 after $3N^3$ successful changes or $15N^3$ trials. The algorithm is terminated if no successful step occurred during the $15N^3$ trials. With the assumption that the number of temperature steps is independent of N the total computing time should scale as N^6. Actually we found a scaling exponent between 6 and 7. Typical CPU times for one run on a DEC alpha workstation were 3.2 h for $N=16$ and 25 h for $N=22$.

The minimizing configurations can be found starting from completely random initial states, but this requires a relatively large initial value of T_s and therefore very long runs. For this reason we started in almost all cases from a configuration that had been obtained as a minimum for other parameter values. It is partly randomized during the first phase of the algorithm by applying an appropriate initial control temperature so that a large fraction of proposals is accepted. By testing in some cases different starting configurations we took care not to bias the final result by a prejudiced initial guess.

III. RESULTS AND DISCUSSION

A. Magnetization structure

As our standard values of the thermodynamic parameters we chose $m^*=\sqrt{m^2/\sigma^3\epsilon}=1.5$, $T^*=k_BT/\epsilon=2.25$, and $\rho^*=\rho\sigma^3=0.94$. This leads to a thermodynamic state that, within the present density-functional theory approximation, lies deep in the ferromagnetic liquid phase. In view of the numerical challenges described in Sec. II B we have examined system sizes $L^*=L/\sigma$ between 4.8 and 12 using lattices consisting of $N=10,12,\ldots,24$ sites in each dimension. (Although we used an ordinary workstation our maximum system size is even 30% larger than the system consisting of 22^3 sites examined by Williams and Dunlop [24] on a supercomputer in 1989.)

The result of a minimization run is a three-component vector field $\mathbf{M}(\mathbf{R})$ representing the magnetization structure within the cubic volume. In order to visualize this field we display sections parallel to the faces of the cube with the magnetization projected onto the section plane. Since one component is lost due to this projection the absolute value $|\mathbf{M}(\mathbf{R})|$ cannot be inferred from these figures. We adopt a reference frame that has its origin in the center of the cube. Figure 1(a) shows a section perpendicular to the z axis at $z^*=z/\sigma=0.18\simeq 0$, i.e., close to the center of the cube, for $L^*=7.2$ and $N=20$. The overall picture is that of a vortex of closed magnetization lines circulating around the z axis. In this context it is interesting to note that clusters of some 10 to 100 dipolar particles also exhibit a vortex structure at low temperatures [33,34]. This structure leads to div $\mathbf{H}=0$ for the resulting magnetic field $\mathbf{H}$. A closer look at the structure in Fig. 1(a) reveals that it may be described as composed of four domains with an approximately constant magnetization separated by broad domain walls along the diagonals of the square within which the direction of $\mathbf{M}$ changes continu-

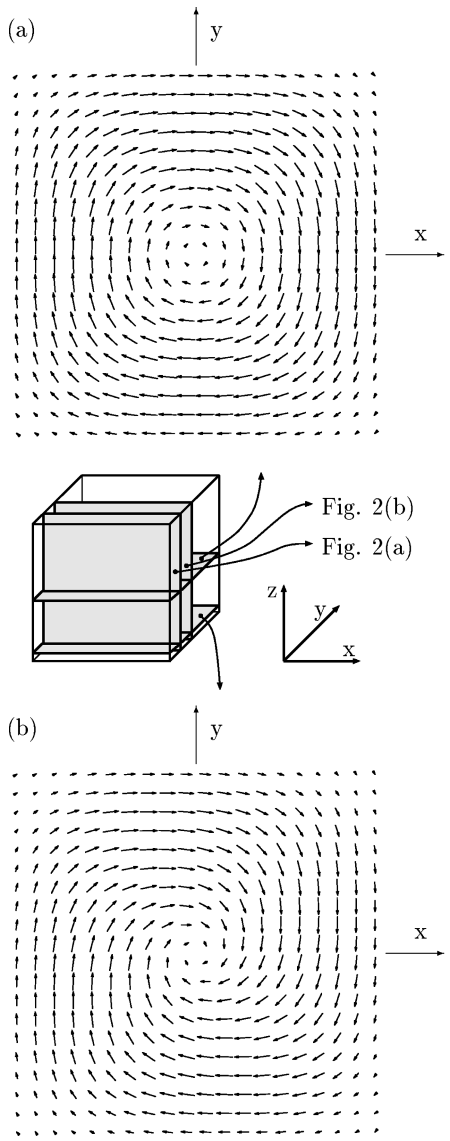

FIG. 1. Sections perpendicular to the z axis through the magnetization structure of a ferromagnetic liquid in a cubic volume (for $L^*=7.2$ and $N=20$); (a) section plane $z^*=0.18$ near the midplane, (b) section plane $z^*=-3.06$ near the bottom. Here and in the following the arrows represent projections onto the section plane of the local magnetization (at the midpoint of the arrows), which is the thermal average of the dipole moments of particles at this point.

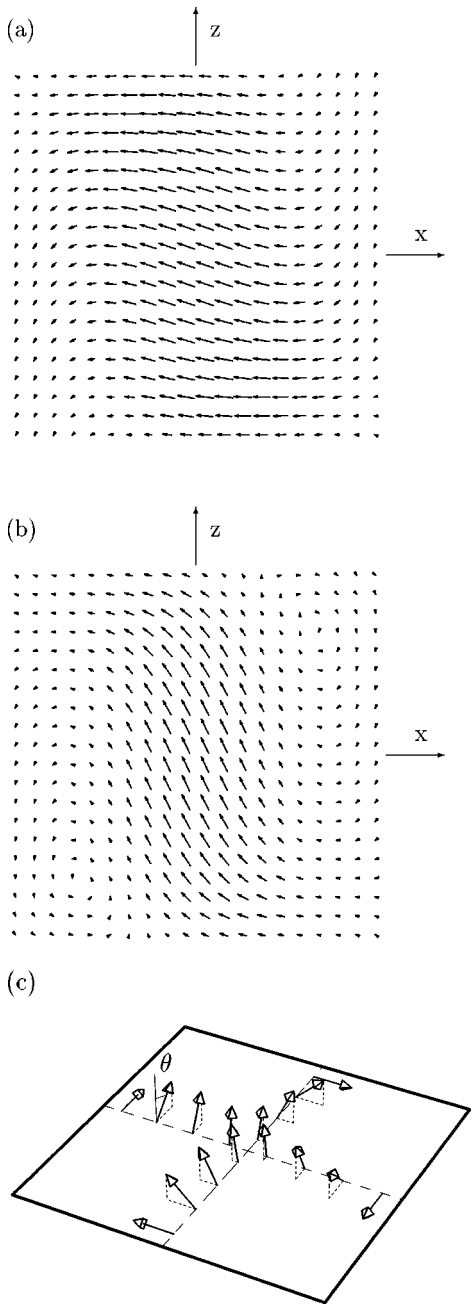

FIG. 2. The same as in Fig. 1, but sections perpendicular to the y axis; (a) $y^*=-1.62$, (b) $y^*=-0.54$. The schematic drawing in (c) demonstrates the mechanism of the ''escape into the third dimension,'' which avoids the formation of a topological line defect along the z axis. θ denotes the polar angle of the magnetization. (The increase of θ to values larger than $\pi/2$ close to the sample edges [see Fig. 4(b)] is not shown.)

ously. This configuration resembles the triangular structure that has been found to be the most stable structure under the constraint of *sharp* domain walls [20]. A similar structure has also been found to be the most favorable one in cubic magnetite particles just above the critical single-domain size, while more complicated structures occur in this case for larger particles [24,25]. In a section near the bottom of the cube [$z^*=-3.06\simeq -L^*/2$, Fig. 1(b)] the domain walls are slightly shifted off the diagonals into the direction opposite to the circulation. The reverse situation is found near the top. However, in contrast to the triangular structure studied in Ref. [20], the magnetization is not confined to a plane. As can be seen in the sections perpendicular to the y axis in Fig. 2 there is a nonvanishing z component, leading to an ''escape into the third dimension,'' which is particularly pronounced near the vortex axis [Figs. 2(b) and (c)]. This mechanism avoids the formation of a topological defect along the z axis. This is in accordance with general considerations showing that line singularities are topologically unstable in a system of three-component spins in three spatial dimensions [35], which means that they can always be removed by continuous *local* modifications. However, near the top and the bottom faces of the cube the z component decreases in order to avoid a large normal component at the surface that would produce an unfavorable demagnetization

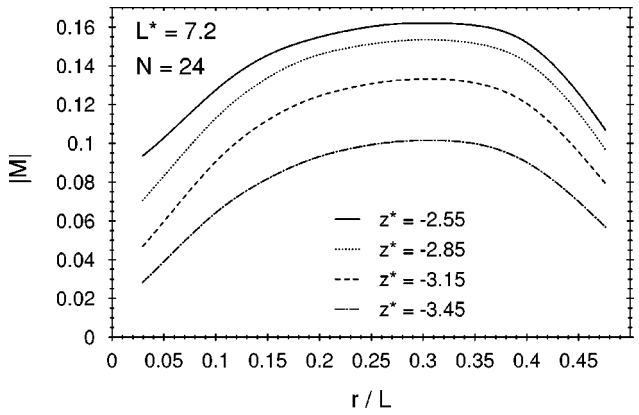

FIG. 3. The absolute value of the dimensionless magnetization near the point defect at the center of the bottom face of the cube (for $L^*=7.2$ and $N=24$). $|\mathbf{M}|$ is plotted as a function of the distance from the z axis along lines parallel to the x or y axis for a series of fixed values of z [compare the case $z\simeq 0$, Fig. 5(a)]. One finds a pronounced decrease of $|\mathbf{M}|$ near the core of the point defect.

field [20]. Thus two topologically stable point singularities near the centers of the bottom and top surfaces are inevitable. A closer look at the magnetization structure reveals a strong decrease of the absolute value of $\mathbf{M}$ in the core of these defects (see Fig. 3). The fact that the size of this less ordered core also scales with the system size underlines the importance of including the absolute value of the magnetization as a minimization parameter. If instead the assumption of constant magnitude of $\mathbf{M}$ were applied, as is usually done in the micromagnetic theory, the defect could not be described correctly even on a mesoscopic scale.

Very similar structures have been found for all values of L and N. In Fig. 4 we compare the ''degree of escape'' for different system sizes with fixed $N=20$. The cosine of the polar angle of $\mathbf{M}$ ($\cos\theta=M_3/M$) is plotted as a function of the distance $r=\sqrt{x^2+y^2}$ from the center along the diagonals (i.e., the lines $x=\pm y$ with $z=\text{const}$) and the center lines (i.e., the lines $x=0$ and $y=0$ with $z=\text{const}$). With the exception of the smallest system the scaling property

$$\mathbf{M}(\mathbf{r}/\sigma,L/\sigma)=\mathbf{M}^{(0)}(\mathbf{r}/L) \tag{26}$$

is approximately fulfilled, so that one can surmise that this holds also in the thermodynamic limit. (Since $\mathbf{M}$ is dimensionless, for a given thermodynamic state it can only depend on $\mathbf{r}/\sigma$ and L/σ.) The function $\mathbf{M}^{(0)}$ represents the global texture in the thermodynamic limit. Near the edges of the cube, i.e., near the corners in the projection plane, there is an escape into the opposite direction, but combined with a strong decrease of the absolute value of the magnetization (see Fig. 5). Upon moving outwards from the center $\cos\theta$ decreases faster along the diagonals than along the center lines, indicating that there is not a circular but rather a square symmetry.

In the inner part of the sample the absolute value $M(\mathbf{R})=|\mathbf{M}(\mathbf{R})|$ (Fig. 5) is approximately constant and independent of L. It decreases near the surface and near the edges. This less ordered surface layer thickens relative to the system size as L decreases. Here, too, scaling with the system size for large L [Eq. (26)] is compatible with the data. In the

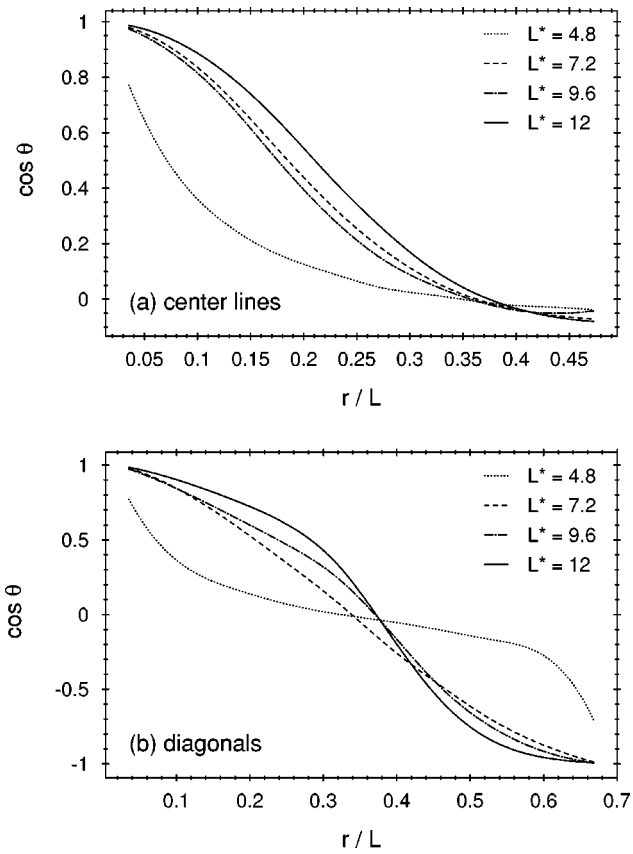

FIG. 4. The cosine of the polar angle of the magnetization ($\cos\theta=M_3/M$) along (a) the center and (b) the diagonal lines within a plane close to the midplane ($z=-a/2$, with the lattice constant $a=L/N$) for $N=20$ and different system sizes L^*. $r=\sqrt{x^2+y^2}$ is the distance from the center of the cube; $r/L\leqslant 0.5$ for the center lines (a) and $r/L\leqslant 1/\sqrt{2}=0.707$ for the diagonals (b). The values of $\cos\theta$ are averaged over the four equivalent sites for each value of r/L. The magnetization ''escapes'' into the positive z direction near the center ($\cos\theta\to 1$), lies in plane ($\cos\theta=0$) near the sample surfaces (center lines), and turns into the negative z direction ($\cos\theta=-1$) near the edges. Except for the smallest system ($L^*=4.8$) the proposed scaling with the system size [see Eq. (26)] is fulfilled approximately, i.e., in the limit $L\gg\sigma$ two master curves evolve, one for the center lines and one for the diagonals.

smallest system we studied ($L^*=4.8$) M decreases also near the center, which indicates a second mode for avoiding a line singularity besides the ''escape into the third dimension.'' This mode appears also for the larger systems near the ferromagnetic-isotropic phase transition and might be induced by the proximity of this transition for $L^*=4.8$ (see Sec. III C). In Fig. 6 we present the average magnetization within each plane parallel to the xy plane $\langle M\rangle_{xy}(z)=N^{-2}\Sigma_{n_1,n_2}M(n_1a,n_2a,z)$ as a function of the height z. Again there is a clear decrease near the surfaces while in the central region $\langle M\rangle_{xy}$ is constant. The average $\langle M\rangle_{xy}$ attains its thermodynamic limit $L\to\infty$ more rapidly than $\cos\theta$ or $M(\mathbf{R})$ (see Figs. 4 and 5). For small L the surface disordered region shrinks on the scale of L but in the thermodynamic limit it remains proportional to L. For large L we find for the excess quantity $\int_{-L/2}^{L/2}dz[\langle M\rangle_{xy}(0)-\langle M\rangle_{xy}(z)]/\langle M\rangle_{xy}(0)\simeq 0.08L$.

As shown in Fig. 7 the minimum value of the free energy

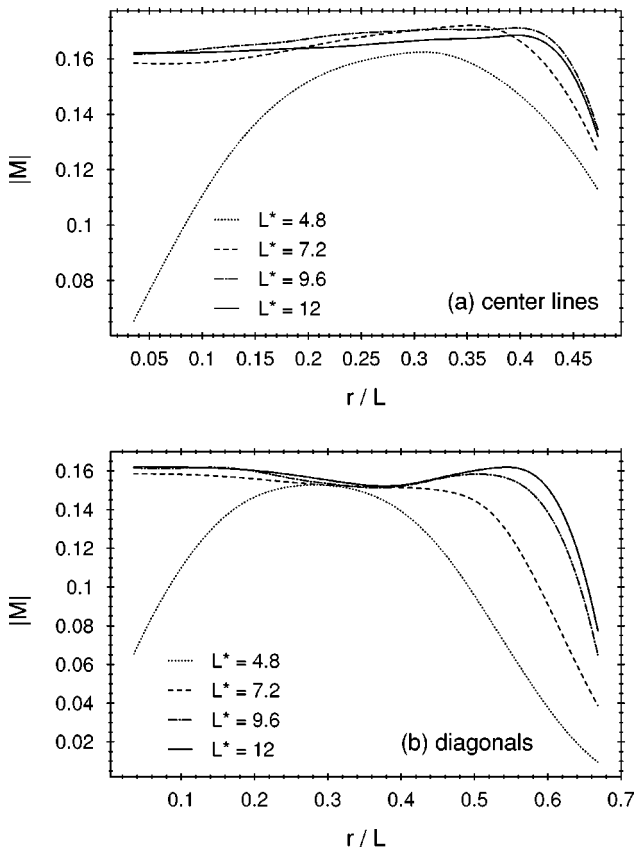

FIG. 5. The absolute value M of the dimensionless magnetization **M** for the same parameters as in Fig. 4 averaged over (a) the four center lines and (b) the four diagonals. With the exception of the smallest system M is approximately constant in the bulk and decreases near the surfaces. For $L \gg \sigma$ the behavior turns into a single master curve consistent with the proposed scaling [Eq. (26)].

density $f_{if}^{*}=(F_{if}/L^{3})(\sigma^{3}/\epsilon)$ exhibits a relatively strong, oscillatory dependence on the lattice constant $a=L/N$ with a decreasing amplitude for increasing values of N. This figure reveals that minima occur when $a/\sigma=L^{*}/N$ is close to the inverse of an integer, which indicates a strong discretization effect. For the larger values of L we could not reach the region where the oscillations have died out, which inhibits a further finite-size analysis. Similar oscillations were found in the spatially averaged value of $M(\mathbf{R})$ and for $L^{*}=4.8$ also in the degree of the rotation out of the plane. The precision to which the minimum value of f_{if}^{*} can be determined by simulated annealing for a given set of parameters is much higher than the discretization effect described above; from the dependence $f_{if}^{*}(T_s)$ we estimate the minimization error to be of the order of 0.01.

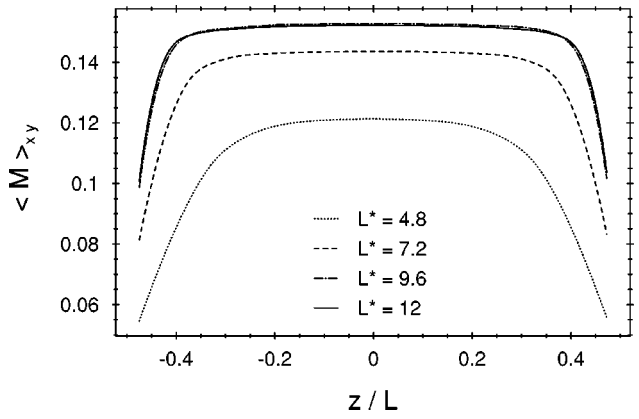

FIG. 6. Averaged absolute value $\langle M\rangle_{xy}$ of the magnetization within the planes $z=$ const for $N=20$ and several system sizes. It is constant in the inner part of the sample and decreases near the bottom and top surfaces. The size of the disordered region remains proportional to L for large L.

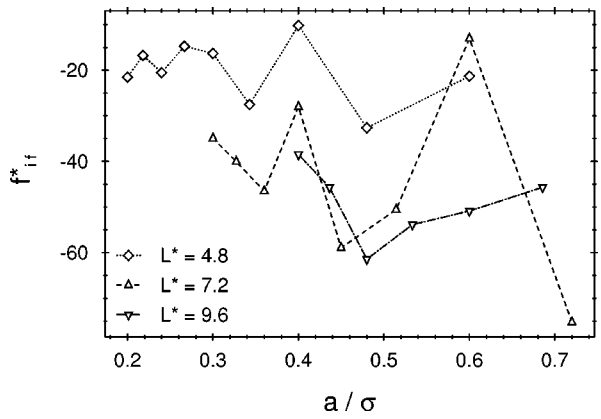

FIG. 7. Reduced free energy difference between the isotropic and the ferromagnetic phase $f_{if}^{*}=(F_{if}/L^{3})(\sigma^{3}/\epsilon)$ as a function of the lattice constant $a/\sigma=L^{*}/N$ of the discretization mesh for three system sizes. The finite lattice constant induces minima (maxima) near the points where the inverse $\sigma/a=N/L^{*}$ is an integer (one-half plus an integer). These oscillations die out for $a\to 0$.

B. Domain walls

In solid ferromagnets the walls between adjacent domains have a microscopic thickness (i.e., it does not scale with the system size) which is determined by the competition between the exchange energy resulting from the spin coupling and the anisotropy energy due to the lattice structure that causes easy axes for the magnetization. Since there is no such lattice anisotropy in liquid ferromagnets de Gennes and Pincus [22] surmised that consequently there are also no domain walls. Below we shall argue that in the case of cubic samples as considered here the thickness of the domain walls is proportional to the system size and thus diverges in the thermodynamic limit. Thus one is left with a question of terminology whether one still speaks of walls, but certainly the behavior is qualitatively different from that in solids.

In order to analyze the properties of the fluid domain walls in the finite cube we consider the behavior of the dimensionless magnetization **M** along straight paths normal to the wall. Along these paths **M** changes continuously between the magnetization directions of the adjacent domains. In the present case these domains have the quasitriangular structure indicated in Fig. 1(a) so that the orientational order between neighboring domains differs by an angle of $\pi/2$. Except near the vortex axis we find a Néel type of wall, i.e., the magnetization vector rotates mainly within the plane spanned by the asymptotic orientations deep inside the adjacent domains; in Fig. 1(a) this is the xy plane. In contrast, in bulk solid ferromagnets one usually observes Bloch walls with the magnetization vector rotating out of plane on a cone around

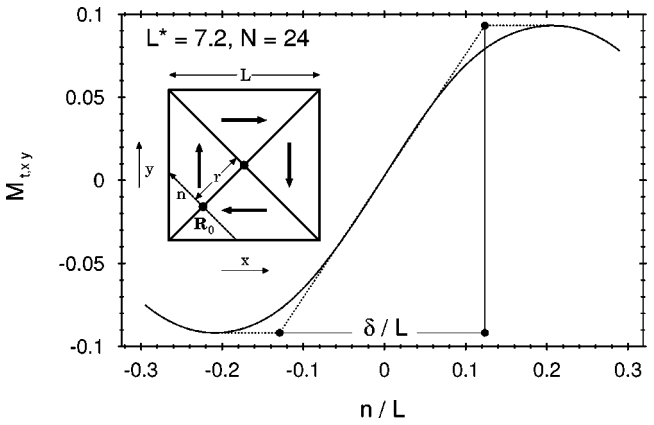

FIG. 8. Variation of the transversal magnetization component $M_{t,xy}=(M_1+M_2)/\sqrt{2}$ upon traversing the domain wall along a normal to the wall through the point $\mathbf{R}_0/\sigma=(-1.95,-1.95,-0.15)$ (see the inset) for $L^*=7.2$ and $N=24$ [compare Fig. 1(a)]. This is the component that characterizes the difference of the magnetization directions of the adjacent domains. Our definition of the wall thickness δ can be inferred from the figure. Here $r/L=0.38$.

the wall normal [36]; only in thin solid films [36] and small particles [24] Néel walls do occur too. In Fig. 8 the relevant transversal component $M_{t,xy}=(M_1+M_2)/\sqrt{2}$ is shown as a function of the normal coordinate n.

We define the wall thickness δ as the distance between the points where the tangent to the curve at its inflection point reaches the extreme values of $M_{t,xy}$ (see Fig. 8). The dependence of δ on the distance r of the wall normal from the center of the cube is displayed in Fig. 9 (all paths lie in the plane $z=-a/2$, i.e., close to the center of the cube). The wall thickness decreases near the edge of the cube where the normal paths hardly reach the region of homogeneous magnetization (see Fig. 1). The thickness increases near the center $r=0$ due to the ''escape'' region [see Fig. 2(c)]. However, it is approximately constant in the range $r/L=0.2,\ldots,0.35$ and there is no monotonic trend as a function of the number of lattice sites. Its dependence on the system size L is analyzed in Fig. 10. Here we selected the values of δ at (or, due to the discrete lattice, close to) $r/L=1/2^{3/2}$ corresponding to half the distance between the center and the edge. For each size L we display the results obtained for different values of N which render an estimate of the uncertainty caused by the finite lattice constant $a=L/N$. A slight decrease of δ/L with increasing L indicates that the domains are getting sharper. However, most probably the data can be extrapolated to a finite limit of δ/L for $L\to\infty$, which would be in accordance with the proposed scaling behavior in Eq. (26).

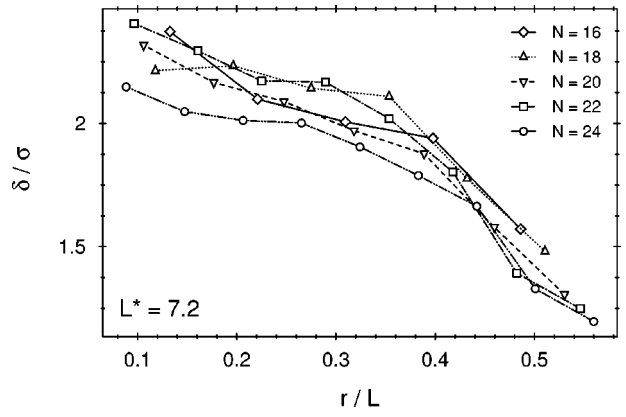

FIG. 9. Dependence of the domain wall thickness δ on the distance r from the center of the plane $z=-a/2\simeq 0$ (i.e., close to the midplane) for $L^*=7.2$ and different numbers of lattice points N, averaged over the four equal walls in the cube (see Fig. 8). In the medium range of r the thickness δ depends only weakly on r and N, while near the center and edges δ is influenced by the escape of the orientation into the z direction and the vicinity of the surfaces, respectively.

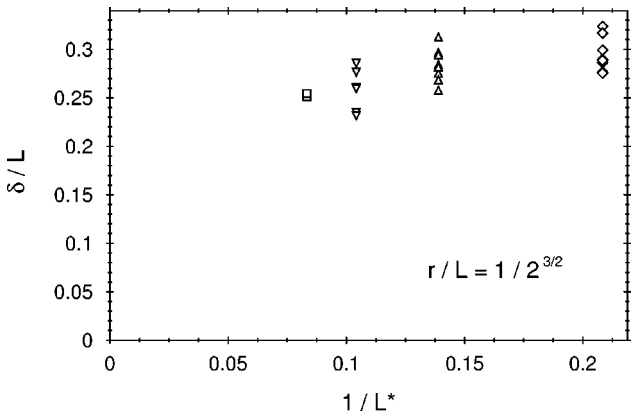

FIG. 10. The wall thickness at half distance between the center and the edges of the cube as a function of the system size L. The different points at the same L correspond to different lattice constants. (From top to bottom: $L^*=4.8$, $N=10,12,14,16,20,18,22,24$; $L^*=7.2$, $N=14,12,18,10,22,16,20,24$; $L^*=9.6$, $N=18,14,16,24,20,22$; $L^*=12$, $N=22,20$.) The extrapolation to $1/L=0$ suggests a finite value of δ/L in the thermodynamic limit.

C. Temperature dependence and critical point

Starting from the standard value $T^*=k_BT/\epsilon=2.25$ used up to here we have increased the temperature at the fixed density $\rho^*=0.94$ in order to examine the structural changes upon approaching the ferromagnetic-isotropic transition. We have chosen $N=16$ and studied the system sizes $L^*=4.8$ and $L^*=9.6$. The spatially averaged absolute value of the magnetization decreases and finally vanishes at a temperature $T_c(L)$ in accordance with the inherent mean field approximation (see Fig. 11). (We define the finite-size critical temperature as the limiting temperature above which no configurations with a negative free energy difference F_{if} are found by the minimization algorithm.) As expected this finite-size (strictly speaking quasi-) critical temperature is lower for smaller systems. From Eq. (7.10) in Ref. [11] we infer $T_c^*(L\to\infty)=3.04$ for the parameters used here. The evolution of the magnetization structure is analyzed in Figs. 12 and 13 for $L^*=9.6$. The escape into the z direction near the vortex axis is strongly reduced at higher temperatures (Fig. 12) while the absolute value of the magnetization in this region decreases more rapidly than for intermediate values of r/L (Fig. 13). Thus a column of less ordered fluid develops around the vortex axis. These effects are even more pronounced in the smaller system, as has been already suggested by Figs. 4 and 5. Furthermore Fig. 13 demonstrates that the surface layer with reduced orientational order thick-

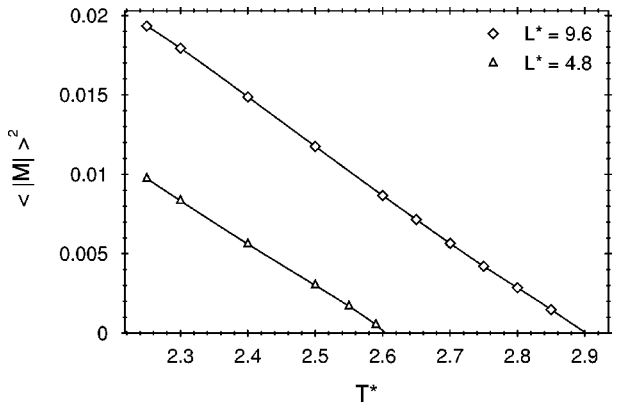

FIG. 11. The squared spatially averaged order parameter $\langle|\mathbf{M}|\rangle^2=[N^{-3}\Sigma_{\mathbf{R}}|\mathbf{M}(\mathbf{R})|]^2$ decreases linearly with increasing temperature T^*. It vanishes at a critical temperature $T_c(L)$, which depends on the system size. This linear behavior holds even outside the close vicinity of $T_c(L)$ where it has to be so due the inherent mean-field character of the present theory.

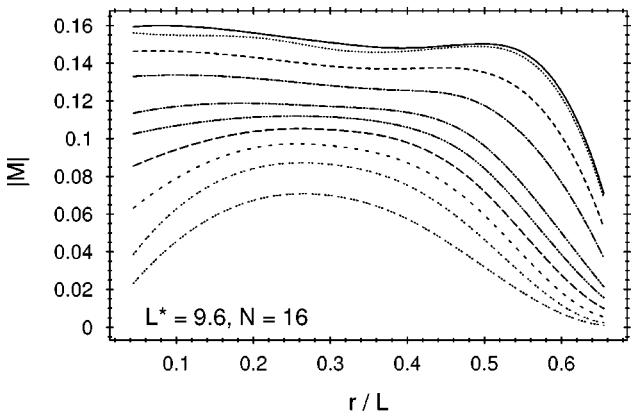

FIG. 13. The absolute value of the magnetization along the diagonal lines (for fixed $z=-a/2$) at various temperatures. The different line styles correspond to the same temperatures as in Fig. 12. Near the phase transition $T_c^*(L^*=9.6)=2.89$ the orientational order is particularly reduced near the vortex axis and in a surface layer of increasing thickness.

ens, which is a consequence of the increasing correlation length upon approaching the phase transition. The domain wall thickness as defined in the preceding subsection also increases slightly but this change is smaller than the uncertainty caused by the finite lattice constant.

IV. EXTERNAL FIELD

Up to now all results refer to zero external field. If an external field is applied the dipolar particles tend to align along the field direction. The resulting transition from the inhomogeneous zero-field configuration to the homogeneously magnetized state in the presence of strong fields can also be examined within the present approach.

The field destroys the equivalence of the three perpendicular directions of the cubic axes. [One should keep in mind that below $T_c(L)$ this equivalence is also *spontaneously* broken in zero field.] We have applied the field normal to the surfaces of the cube either parallel or perpendicular to the spontaneously chosen vortex axis of the zero-field configuration, which was used as an initial guess for the minimization algorithm. The most stable configurations were found when the external field is parallel to the vortex axis. (In principle, equivalent but rotated configurations should be obtained if at the beginning of the algorithm the field is applied perpendicular to this axis. Since, however, only a medium value for the initial control temperature was employed, for this latter choice of the initial guess the system could not reach the equilibrium structure, which in this case differs significantly from the initial configuration.) The relative stability of the resulting configurations can be judged on the basis of the corresponding value of the free energy. A typical result is depicted in Figs. 14 and 15. The section parallel to the xy plane, i.e., perpendicular to the external field, exhibits smaller absolute values of the magnetization components orthogonal to the field direction than for $H=0$ (Fig. 14), but the structure is very similar. On the other hand there is a substantial increase of the magnetization component parallel to the field as shown in the sections $y=$ const in Fig. 15. Thus the overall structure is essentially preserved, but at each point the magnetization is rotated into the field direction by a certain amount. This demonstrates that this behavior, which was anticipated in Ref. [20], corresponds indeed to the equilibrium configuration. If the field is sufficiently strong the vortex structure is lost at a critical field strength H_c. This is shown in Fig. 16 by the field dependence of the averaged parallel component $\langle M_{\parallel}\rangle = N^{-3}\Sigma_{\mathbf{R}}M_3(\mathbf{R})$ and of the angular component $\langle M_{\varphi}\rangle = N^{-3}\Sigma_{\mathbf{R}}\mathbf{e}_{\varphi}(\mathbf{R})\cdot\mathbf{M}(\mathbf{R})$, where $\mathbf{e}_{\varphi}(\mathbf{R})=(R_2,-R_1,0)/|\mathbf{R}|$. Below H_c the parallel component increases approximately linearly [20] while the angular component decreases and vanishes at H_c (apparently linearly in H_c-H). The absolute value of $\mathbf{M}$ increases almost homogeneously over the sample. A surface layer of lower magnetization is preserved even in the presence of strong fields. Above H_c the increase of $\langle M_{\parallel}\rangle$ is only due to the increase of $|\mathbf{M}|$ and will saturate in the limit $H\to\infty$.

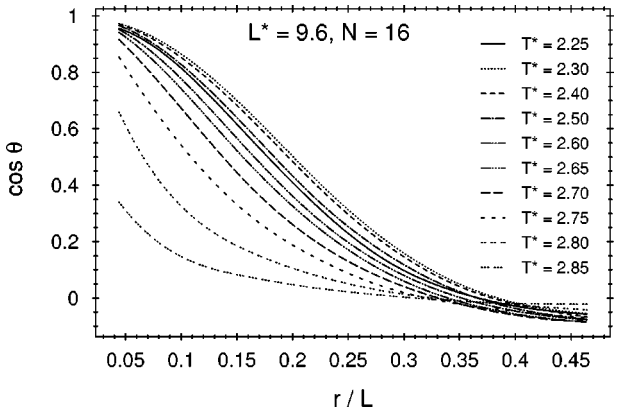

FIG. 12. The polar angle of $\mathbf{M}$ [see Figs. 2(c) and 4] along the central lines near the midplane (fixed $z=-a/2$ as in Fig. 4) as a function of the temperature for $L^*=9.6$ and $N=16$. The escape near the vortex axis reduces upon approaching the critical point $T_c^*(L^*=9.6)=2.89$.

These results should be compared with those of a micromagnetic calculation for isotropic *spheres* by Aharoni and Jakubovics [37]. They were intended as a first step in modeling amorphous solid ferromagnets, but due to the assump-

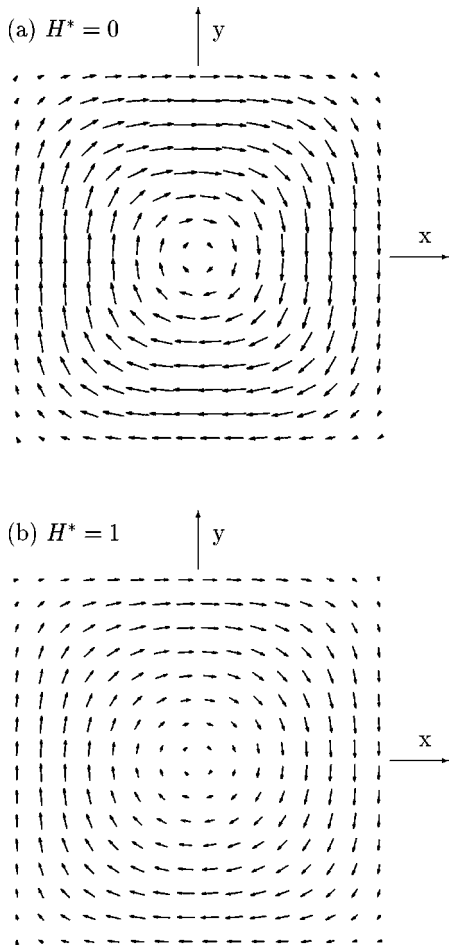

FIG. 14. Sections orthogonal to the field direction through the magnetization structure for $L^*=9.6$ and $N=16$ at $z^*=-0.9$ (a) without and (b) with an external field $H^*=H\sqrt{\sigma^3/\epsilon}=1$ applied in the z direction. The scale factor that determines the lengths of the arrows is the same in both parts of this figure and also in Fig. 15. The transversal components of the magnetization are reduced by the field but the overall feature of the inhomogeneous structure is preserved.

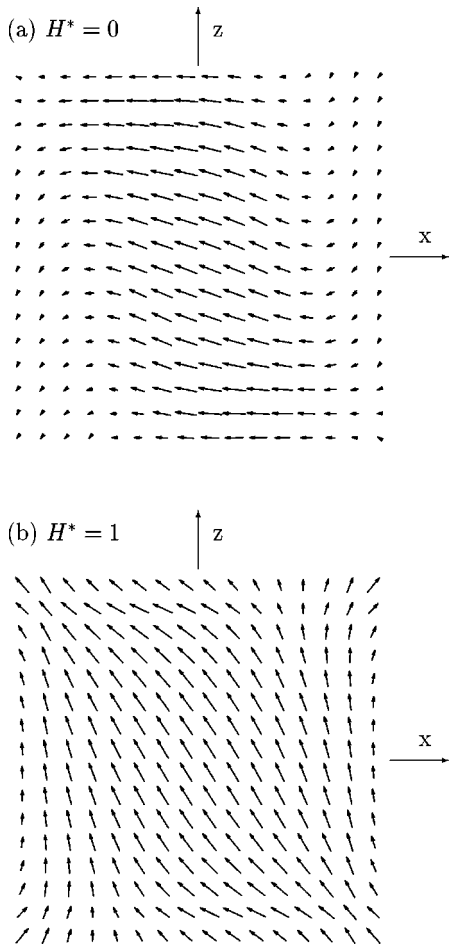

FIG. 15. Vertical sections perpendicular to the y axis and thus parallel to the field direction through the same magnetization structures as in Fig. 14 for $y^*=-2.1$. At this distance of the plane from the center the z component of the magnetization in zero field is only small, while the external field induces a large z component everywhere.

tion of a vanishing anisotropy constant they should also be of interest for liquid ferromagnets. These authors find a vortex structure with the axis parallel to the external field too. In the center of the vortex the magnetization points into the field direction, also for $H\rightarrow 0$. However, for the cube this contribution to the net magnetization is compensated by the opposite orientation of the magnetization near the edges [see Fig. 4(b)]. This implies that for cubes $\langle M_{\parallel}\rangle \simeq 0$ for $H\rightarrow 0$, whereas for spheres a spontaneous net magnetization $\langle M_{\parallel}\rangle(H\rightarrow 0^{+})=-\langle M_{\parallel}\rangle(H\rightarrow 0^{-})\neq 0$ remains in the limits $H\rightarrow 0^{\pm}$. This discontinuity at $H=0$ yields an infinite zero field susceptibility. Thus spontaneous liquid ferromagnetism should be easier to detect by macroscopic magnetization measurements in spherical than in cubic samples.

The same transition between an inhomogeneous and a nearly homogeneous state arises when the external field is kept fixed and the temperature is varied. As shown in Fig. 17 the angular magnetization component decreases with increasing T and vanishes at a critical temperature $T_c(H)$, which is lower than $T_c(H=0)$ (compare Fig. 11). The par-

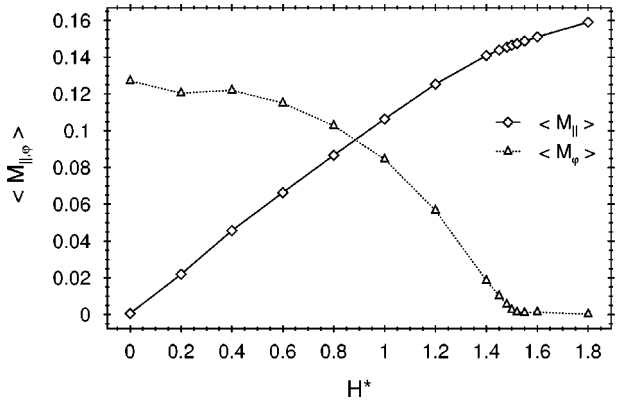

FIG. 16. Dependence of the averaged longitudinal magnetization component $\langle M_{\parallel}\rangle$ and the averaged angular component $\langle M_{\varphi}\rangle$ on the field strength ($L^*=9.6$, $N=16$, $T^*=2.25$). The angular component decreases for increasing H^* and vanishes seemingly linearly at $H_c^*\simeq 1.50$. Below H_c^* the parallel component increases approximately linearly and crosses over towards saturation for $H^*>H_c^*$. Above H_c^* the sample has an approximately homogeneous magnetization. Compare Fig. 11 in Ref. [20].

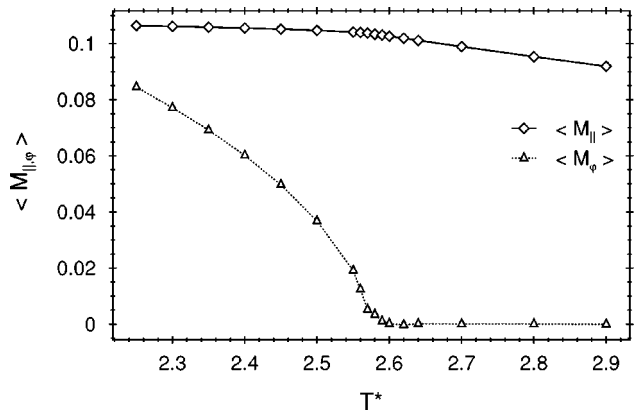

FIG. 17. The same magnetization components as in Fig. 16 for fixed $H^*=1$ as a function of temperature ($L^*=9.6$, $N=16$). There is a transition from a vortex structure to an almost homogeneous magnetization at $T_c^*(H^*)\simeq 2.65$. Compare Fig. 12 in Ref. [20].

allel component is nearly constant below T_c and decreases gradually above T_c where the sample is almost homogeneously magnetized. Our previous work [20] as well as Ref. [38] predict a kink in the curve $M_\parallel(T)$ and the constant value $\mathcal{M}(T<T_c)=H/(4\pi D)$ with the demagnetization factor D. In the present units, using $D=1/3$ for the cube, this would mean $M(T<T_c)=(3/4\pi)^{3/2}H/(\rho m)\simeq 0.0827$ for the parameters used in Fig. 17. Both features have also been observed in *ellipsoidal* samples of a solid dipolar Ising ferromagnet [39]. Obviously the present theory yields a higher plateau value of the magnetization and a rounding of the kink at the phase transition. One also observes that the angular component vanishes linearly at the critical point, as in Fig. 16, but in contrast to the simplified model used in Ref. [20]. We surmise that these differences are due to the fact that for a *cube* the assumption adopted in Refs. [38] and [20] of a homogeneous magnetization $M_\parallel$ in both phases is not fulfilled. Another possible source for this discrepancy could be the finite size of the systems we examined.

V. SUMMARY

Based on density-functional theory we have obtained the following main results for the long-ranged orientational order of a dipolar liquid confined to a cube:

(1) The equilibrium magnetization configuration corresponds to a predominantly planar vortex structure, which can be viewed as being composed of four triangular domains separated by thick domain walls along the diagonal planes of the cube. Near one of the symmetry axes of the cube chosen spontaneously the magnetization escapes into the third dimension in order to avoid a topological line singularity (Figs. 1, 2, and 4).

(2) Point defects arise at the centers of the top and bottom face of the cube. The absolute value $|\mathbf{M}|$ of the magnetization is reduced inside the cores of these defects (Fig. 3) whose sizes scale with the system size. Therefore an appropriate description of the structure requires to take the spatial variation of $|\mathbf{M}|$ into account.

(3) Near the surfaces there is a layer of reduced orientational order (Figs. 5 and 6).

(4) The domain walls (Fig. 8) are mainly of the Néel type, i.e., upon traversing the wall the magnetization rotates within the plane spanned by its asymptotic directions deep inside the adjacent domains. The size dependence of the wall thickness (Fig. 10) and of other features of the configurations are compatible with the scaling behavior formulated in Eq. (26).

(5) The ferromagnetic order vanishes at a critical temperature that depends on the system size (Fig. 11). Upon increasing the temperature the ''escape'' region near the vortex axis is gradually replaced by a column of disordered fluid (Figs. 12 and 13).

(6) In weak external fields normal to the surfaces of the cube the vortex axis is aligned parallel to the field direction and the overall structure is similar to the one in zero field (Figs. 14 and 15). For stronger fields the magnetization is rotated increasingly into the field direction until a transition to an approximately homogeneously magnetized state takes place at a critical field strength beyond which the vortex structure is lost (Fig. 16). In an external field the magnetization components normal to the field direction vanish linearly upon approaching a critical temperature (Fig. 17).

Recently metallic liquid ferromagnets have been discovered in undercooled CoPd alloys [27–29]. For the formation of the ferromagnetic order of these materials short-ranged exchange interactions play an important role. However, in addition dipolar interactions are also present and, as in solid ferromagnets, are essential in forming the domain structure. Therefore for these systems we expect strong similarities to the behavior of dipolar fluids as discussed in this work. Up to now these undercooled liquid alloys have been prepared only as electromagnetically suspended spherical samples. One can speculate that the domain structure within a sphere has a vortex axis too, but no domain walls due to the higher symmetry compared to a cube. Our analysis indicates that an experimental study of these structures (e.g., by using magnetic neutron or x-ray tomography [40]) would certainly be very rewarding. Thus to our knowledge to date there are no experimental results that could be directly compared to our theory. However, we stress that the present method is generally applicable for studying the structure and the phase behavior of orientationally ordered liquids exposed to external fields such as, e.g., mixtures of magnetic and nonmagnetic fluids in external magnetic fields, which exhibit interesting drop shapes and surface instabilities [41–43].

ACKNOWLEDGMENT

One of us (S.D.) acknowledges helpful discussions with D. Thouless.

[1] D. Wei and G. N. Patey, Phys. Rev. Lett. **68**, 2043 (1992).
[2] D. Wei and G. N. Patey, Phys. Rev. A **46**, 7783 (1992).
[3] J. J. Weis, D. Levesque, and G. J. Zarragoicoechea, Phys. Rev. Lett. **69**, 913 (1992).
[4] J. J. Weis and D. Levesque, Phys. Rev. E **48**, 3728 (1993).
[5] M. J. Stevens and G. S. Grest, Phys. Rev. E **51**, 5962 (1995).
[6] M. J. Stevens and G. S. Grest, Phys. Rev. E **51**, 5976 (1995).
[7] K. Sano and M. Doi, J. Phys. Soc. Jpn. **52**, 2810 (1983).
[8] H. Zhang and M. Widom, Phys. Rev. E **49**, R3591 (1994).
[9] D. Wei, G. N. Patey, and A. Perera, Phys. Rev. E **47**, 506 (1993).
[10] B. Groh and S. Dietrich, Phys. Rev. Lett. **72**, 2422 (1994); **74**, 2617 (1995).
[11] B. Groh and S. Dietrich, Phys. Rev. E **50**, 3814 (1994).
[12] M. E. van Leeuwen and B. Smit, Phys. Rev. Lett. **71**, 3991 (1993).
[13] J. J. Weis and D. Levesque, Phys. Rev. Lett. **71**, 2729 (1993).
[14] D. Levesque and J. J. Weis, Phys. Rev. E **49**, 5131 (1994).
[15] S. C. McGrother and G. Jackson, Phys. Rev. Lett. **76**, 4183 (1996).
[16] R. P. Sear, Phys. Rev. Lett. **76**, 2310 (1996).
[17] R. van Roij, Phys. Rev. Lett. **76**, 3348 (1996).
[18] M. A. Osipov, P. I. C. Teixeira, and M. M. Telo da Gama, Phys. Rev. E **54**, 2597 (1996).
[19] M. Widom and H. Zhang, Phys. Rev. Lett. **74**, 2616 (1995).
[20] B. Groh and S. Dietrich, Phys. Rev. E **53**, 2509 (1996).
[21] R. B. Griffiths, Phys. Rev. **176**, 655 (1968).
[22] P. G. de Gennes and P. A. Pincus, Solid State Commun. **7**, 339 (1969).
[23] W. F. Brown, Jr., *Micromagnetics* (Krieger, Huntington, 1978).
[24] W. Williams and D. J. Dunlop, Nature (London) **337**, 634 (1989).
[25] A. J. Newell, D. J. Dunlop, and W. Williams, J. Geophys. Res. **98**, 9533 (1993).
[26] B. Groh and S. Dietrich, Phys. Rev. Lett. **79**, 749 (1997).
[27] D. Platzek, C. Notthoff, D. M. Herlach, G. Jacobs, D. Herlach, and K. Maier, Appl. Phys. Lett. **65**, 1723 (1994).
[28] J. Reske, D. M. Herlach, F. Keuser, K. Maier, and D. Platzek, Phys. Rev. Lett. **75**, 737 (1995).
[29] T. Albrecht, C. Bührer, M. Fähnle, K. Maier, D. Platzek, and J. Reske, Appl. Phys. A: Solids Surf. **65**, 215 (1997).
[30] P. Frodl and S. Dietrich, Phys. Rev. A **45**, 7330 (1992); Phys. Rev. E **48**, 3203 (1993).
[31] S. Klapp and F. Forstmann, Europhys. Lett. **38**, 663 (1997); J. Chem. Phys. **106**, 9742 (1997).
[32] W. H. Press, B. P. Flannery, S. A. Teukolsky, and W. T. Vetterling, *Numerical Recipes* (Cambridge University Press, Cambridge, 1989); simulated annealing is a stochastic numerical method to find the minimum of a complicated function of many variables and thus should be distinguished from a Monte Carlo simulation.
[33] H. B. Lavender, K. A. Iyer, and S. J. Singer, J. Chem. Phys. **101**, 7856 (1994).
[34] D. Lu and S. J. Singer, J. Chem. Phys. **103**, 1913 (1995).
[35] N. D. Mermin, Rev. Mod. Phys. **51**, 591 (1979).
[36] A. Hubert, *Theorie der Domänenwände in geordneten Medien*, Lecture Notes in Physics, edited by J. Ehlers, K. Hepp, and H. A. Weidenmüller (Springer, Berlin, 1974), Vol. 26.
[37] A. Aharoni and J. P. Jakubovics, J. Magn. Magn. Mater. **83**, 451 (1990).
[38] P. J. Wojtowicz and M. Rayl, Phys. Rev. Lett. **20**, 1489 (1968).
[39] R. Frowein and J. Kötzler, Z. Phys. B **25**, 279 (1976).
[40] G. Schmahl, P. Guttmann, D. Raasch, P. Fischer, and G. Schütz, Synchrotron Radiation News **9**, 35 (1996).
[41] J. H. E. Promislow and A. P. Gast, Phys. Rev. E **56**, 642 (1997).
[42] D. P. Jackson, R. E. Goldstein, and A. O. Cebers, Phys. Rev. E **50**, 298 (1994).
[43] M. Seul and D. Andelman, Science **267**, 476 (1995).